Physics Letters A 534 (2025) 130241

Contents lists available at ScienceDirect

Physics Letters A

journal homepage: www.elsevier.com/locate/pla

Discussion

Unidirectional amplified reflections based on four-wave mixing and spontaneously generated coherence

Yue Geng [a], Chen Peng [a], Xinfu Zheng [a], Dong Yan [a], Hanxiao Zhang [a], Jinhui Wu [b,*], Hong Yang [a,*]

[a] School of Physics and Electronic Engineering, Hainan Normal University, Haikou 571158, China
[b] Center for Quantum Sciences and School of Physics, Northeast Normal University, Changchun 130024, China

ARTICLE INFO

Communicated by S. Khonina

ABSTRACT

The ability to realize unidirectionality and signal amplification in the same device has become an urgent demand, with the increasingly high requirements for integrating signal processing devices. We propose a feasible scheme to achieve amplified unidirectional reflection in a coherent active atomic system via four-wave mixing (FWM) and spontaneously generated coherence (SGC), based on symmetry breaking caused by the spatially linear modulation of coupling on symmetry breaking caused by the spatially linear modulation of coupling fields. Specifically, a narrowed and amplified unidirectional reflection band can be generated in the weak-coupling regime of light-atom interactions with the combination of FWM and SGC, which can be modulated by the relative phase ϕ and dipole angle θ. This high and narrow band yields low out-of-band noise, which can prove more advantageous for many on-chip functionalities.

1. Introduction

All-optical diodes, isolators and circulators, serve as fundamental elements in integrated quantum circuits have attracted intensive research, for its important potential applications in quantum information technology [1–5]. High-performance nonreciprocal amplification is an essential functionality in integrated photonic circuits, which can simultaneously amplify the weak signal output by the quantum system and isolate the sensitive quantum system from the backscattered external noise [6,7]. However, under normal conditions, the nonreciprocal and amplified devices are independent of each other in the information network, each performing its own function separately. It is an urgent demand to simultaneously manipulate optical nonreciprocity and signal amplification in the same device, for the increasingly high requirements of integrating signal processing devices.

Up to now, various promising physical systems have been proposed for nonreciprocal optical amplification. Such as Josephson circuit [8,9], non-Hermitian time Floquet systems [10,11], and parity-time symmetric structures [12,13], and these seem to be the intensively studied fields in nonreciprocal amplification and asymmetric lasing of active systems. Additionally, in silicon photonic device technologies, the nonreciprocal amplified light signal within silicon waveguides based Brillouin scattering is central to the development of high-performance photonic devices [14–17]. Cavity optomechanics is also playing an increasingly important role in making and steering on-chip high-performance nonreciprocal devices, including microwave amplification using a cavity magnonic system [18,19], the unidirectional amplification in whispering-gallery cavity [20,21], the nonreciprocal phonon lasing in a coupled cavity system composed of an optomechanical resonator and a spinning resonator [22–24], and others [25–29]. The optical cavity plays an important role in nonreciprocal amplification for its feedback effect, and atoms coupled with the optical cavity are also a feasible regime [30]. However, it is promising to explore more functions and applications by manipulating nonreciprocal amplification in atomic system. The nonreciprocal amplification based on four-level hot atoms by exploiting atomic Doppler shifts opens up a new avenue towards realistic devices based on nonreciprocal amplification [31,32].

Recently, our two works have focused on studying nonreciprocal reflection amplification in a uniform atomic medium, based on the spatial symmetry breaking effect and skillfully designed coherent active

* Corresponding authors.
E-mail addresses: jhwu@nenu.edu.cn (J. Wu), yang_hongbj@126.com (H. Yang).

https://doi.org/10.1016/j.physleta.2025.130241
Received 29 November 2024; Received in revised form 3 January 2025; Accepted 6 January 2025

Available online 13 January 2025

atomic system [33,34]. In Ref. [33], we propose a theoretical model of four-level atoms via four-wave mixing (FWM) to amplify the unidirectional reflection. For the nonlinear effect caused by four laser beams can amplify the probe light locating in the window of electromagnetically induced transparency (EIT), or enhance the optical parametric oscillation [35,36], the FWM process has been applied in studying many quantum interference systems [37–40]. Especially, this nonlinear effect can also be generated through spontaneous six-wave mixing which are studied theoretically and experimentally [41,42]. Another method of generating quantum interference is related to relaxation processes such as spontaneous emission, e.g., vacuum induced coherence (VIC) [43–45], which is also known as spontaneously generated coherence (SGC) [46–51], that can cause the destructive quantum interference between the two or more different quantum pathways [52–54]. SGC effect has been proved by the vacuum-induced quantum beats, that observed by the latest experiment in atomic ensembles [45].

In this paper, we propose a scheme by combining the FWM and the SGC effects together with a spatially linear modulation (SLM) on coupling intensities for enhancing and optimizing unidirectional amplified reflection. It is surprising that high-contrast nonreciprocal reflection can be achieved with one reflectivity approaching 3500 while the other being just 1.4 in a dilute atomic gas, and with low intensity of control fields. After optimizing the relevant parameters, we can further achieve an amplified unidirectional reflection band with one reflectivity exceeding 60 while the other being vanishing for an extremely narrow linewidth of 10 kHz, and meanwhile realize a flexible phase control for reversing the amplified and vanishing reflectivities. This is because the two probe fields are not absorbed due to the EIT effect, while could be amplified enabled by the nonlinear effect caused by FWM, and SGC promises a largely enhanced and phase tunable reflection amplification of the probe field. Different from parity-time symmetry [55–57] and the Kramers-Kronig relation [58–61] as used in typical atomic systems, the unidirectional reflection in our scheme is caused by SLM referring to the linear increase of coupling field intensities with atomic positions. This SLM not only breaks the spatial symmetry of probe susceptibility but also causes the resonance absorption of probe light when incident from the left side due to the weak coupling field. However, the probe light can be well reflected when incident from the right side due to the EIT effect caused by the strong coupling field.

2. Theoretical model and equations

As shown in Fig. 1(a), the cold ^{87}Rb atoms are driven into a four-level double Λ-type system, by two weak probe fields and two strong coupling fields. The probe beams of Rabi frequency (detuning) $\Omega_{p1} = \mathbf{E}_{p1}\cdot\mathbf{d}_{32}/2\hbar$ ($\Delta_{p1} = \omega_{p1} - \omega_{32}$), $\Omega_{p2} = \mathbf{E}_{p2}\cdot\mathbf{d}_{41}/2\hbar$ ($\Delta_{p2} = \omega_{p2} - \omega_{41}$) and the coupling fields of Rabi frequency (detuning) $\Omega_{c1} = \mathbf{E}_{c1}\cdot\mathbf{d}_{31}/2\hbar$ ($\Delta_{c1} = \omega_{c1} - \omega_{31}$), $\Omega_{c2} = \mathbf{E}_{c2}\cdot\mathbf{d}_{42}/2\hbar$ ($\Delta_{c2} = \omega_{c2} - \omega_{42}$) drive the dipole allowed transition $|2\rangle \leftrightarrow |3\rangle$, $|1\rangle \leftrightarrow |4\rangle$, $|1\rangle \leftrightarrow |3\rangle$ and $|2\rangle \leftrightarrow |4\rangle$. The matrix element $\mathbf{d}_{ij} = \langle i|\,\mathbf{d}\,|j\rangle$ is used to denote the dipole moment of transition $|i\rangle$ to $|j\rangle$. Specifically, the energy levels $|1\rangle$ and $|2\rangle$ refer to two close enough states $\left|5S_{1/2}, F=1, m_F=-1\right\rangle$, $\left|5S_{1/2}, F=1, m_F=0\right\rangle$, levels $|3\rangle$ and $|4\rangle$ refer to excited states $\left|5P_{1/2}, F=1, m_F=-1\right\rangle$ and $\left|5P_{1/2}, F=2, m_F=0\right\rangle$ of cold ^{87}Rb atoms' D1 line broken by static magnetic fields, respectively. The homogeneous distribution of cold atoms is displayed in Fig. 1(d), the probe field travels along the x-axis, while the control fields travel vertically along x-axis. It is worth emphasizing that the Doppler broadening can be ignored safely in our cold atomic sample.

With the electric-dipole and rotating-wave approximations, the interaction Hamiltonian of atom-field can be written as

$$\begin{aligned} H_I &= \hbar\left[(\Delta_{c1}-\Delta_{p1})\,|2\rangle\langle 2| + \Delta_{c1}\,|3\rangle\langle 3| + \Delta_{p2}\,|4\rangle\langle 4|\right] \\ &- \hbar[\Omega_{c1}(x)\,|3\rangle\langle 1| + \Omega_{p1}\,|3\rangle\langle 2| + \Omega_{c2}(x)\,|4\rangle\langle 2| + \Omega_{p2}\,|4\rangle\langle 1| + \mathbf{H.c.}] \end{aligned} \tag{1}$$

According to the definition, the density matrix element ρ_{ij} is the product of the probability amplitude of the population between states $|i\rangle$ and $|j\rangle$, and Γ_{ij} denotes the population decay rate from level $|i\rangle$ to level $|j\rangle$. Additionally, $\gamma_{ij} = (\Gamma_{in} + \Gamma_{jn})/2$ is the dephasing rate associated with atomic coherence ρ_{ij}. The above equations are constrained by $\rho_{11} + \rho_{22} + \rho_{33} + \rho_{44} = 1$, conjugate conditions $\rho_{ij} = \rho_{ji}^*$ and the steady-state condition $\dot\rho_{ij} = 0$. Here θ_i $(i = 1, 2)$ is the angle between the two induced dipole moments shown in Fig. 1(a). $\eta_0\sqrt{\Gamma_{31}\Gamma_{32}}\cos\theta_1 e^{i\varphi_1}$ $(\eta_0\sqrt{\Gamma_{41}\Gamma_{42}}\cos\theta_2 e^{i\varphi_2})$ represents the quantum interference effect arising from the cross-coupling between spontaneous emission $|3\rangle \leftrightarrow |1\rangle$ and $|3\rangle \leftrightarrow |2\rangle$ ($|4\rangle \leftrightarrow |1\rangle$ and $|4\rangle \leftrightarrow |2\rangle$), respectively. Note that the existence of SGC requires that dipole moments $\mathbf{d}_{31}(\mathbf{d}_{41})$ and $\mathbf{d}_{32}(\mathbf{d}_{42})$ are not orthogonal, which is denoted by $\eta_0 = 1$ otherwise $\eta_0 = 0$.

Then, by substituting H_I into the master equation of motion for the density operator and using the Weisskopf-Wigner theory of spontaneous emission [49], we obtain the following density matrix elements

$$\begin{aligned}
&\dot\rho_{11} = i\Omega_{c1}^*(x)\rho_{31} - i\Omega_{c1}(x)\rho_{13} + i\Omega_{p2}^*\rho_{41} - i\Omega_{p2}\rho_{14} + \Gamma_{31}\rho_{33} + \Gamma_{41}\rho_{44} \\
&\dot\rho_{12} = [i(\Delta_{c1} - \Delta_{p1}) - \gamma_{12}]\rho_{12} + i\Omega_{c1}^*(x)\rho_{32} - i\Omega_{p1}\rho_{13} + i\Omega_{p2}^*\rho_{42} \\
&- i\Omega_{c2}\rho_{14} - (\eta_0\sqrt{\Gamma_{31}\Gamma_{32}}\cos\theta_1\rho_{33}e^{i\varphi_1} + \eta_0\sqrt{\Gamma_{41}\Gamma_{42}}\cos\theta_2\rho_{44}e^{i\varphi_2}) \\
&\dot\rho_{13} = (i\Delta_{c1} - \gamma_{13})\rho_{13} - i\Omega_{c1}^*(x)\rho_{11} - i\Omega_{p1}^*\rho_{12} + i\Omega_{c1}^*(x)\rho_{33} + i\Omega_{p2}^*\rho_{43} \\
&\dot\rho_{14} = (i\Delta_{p2} - \gamma_{14})\rho_{14} - i\Omega_{p2}^*\rho_{11} - i\Omega_{c2}^*(x)\rho_{12} + i\Omega_{c1}^*(x)\rho_{34} + i\Omega_{p2}^*\rho_{44} \\
&\dot\rho_{22} = i\Omega_{p1}^*\rho_{32} - i\Omega_{p1}\rho_{23} + i\Omega_{c2}^*(x)\rho_{42} - i\Omega_{c2}(x)\rho_{24} + \Gamma_{32}\rho_{33} + \Gamma_{42}\rho_{44} \\
&\dot\rho_{23} = (i\Delta_{p1} - \gamma_{23})\rho_{23} - i\Omega_{c1}^*(x)\rho_{21} - i\Omega_{p1}^*\rho_{22} + i\Omega_{p1}^*\rho_{33} + i\Omega_{c2}^*(x)\rho_{43} \\
&\dot\rho_{24} = (i\Delta_{c2} - \gamma_{24})\rho_{24} - i\Omega_{p2}^*\rho_{21} - i\Omega_{c2}^*(x)\rho_{22} + i\Omega_{p1}^*\rho_{34} + i\Omega_{c2}^*(x)\rho_{44} \\
&\dot\rho_{33} = i\Omega_{c1}(x)\rho_{13} - i\Omega_{c1}^*(x)\rho_{31} + i\Omega_{p1}\rho_{23} - i\Omega_{p1}^*\rho_{32} - \Gamma_{32}\rho_{33} - \Gamma_{31}\rho_{33} \\
&\dot\rho_{34} = [i(\Delta_{p2} - \Delta_{c1}) - \gamma_{34}]\rho_{34} + i\Omega_{c1}(x)\rho_{14} - i\Omega_{p2}^*\rho_{31} \\
&+ i\Omega_{p1}\rho_{24} - i\Omega_{c2}^*(x)\rho_{32}
\end{aligned} \tag{2}$$

By taking into account the field phases required by SGC. We make the standard transformation of the equations as follows: First, the corresponding Rabi frequencies are redefined as $\Omega_{pi} = G_{pi}e^{i\varphi_{pi}}$ $(G_{pi} = G_{p0i}\sin\theta_i)$ and $\Omega_{ci} = G_{ci}e^{i\varphi_{pi}}$ $(G_{ci} = G_{c0i}\sin\theta_i)$, $i = 1, 2$, where G_{pi} and G_{ci} are all real numbers; then we redefine atomic variables in Eq. (2) as $\rho_{ii} = \sigma_{ii}$, $\rho_{12} = \sigma_{12}e^{i(\varphi_{p1}-\varphi_{c1})}$, $\rho_{21} = \sigma_{21}e^{i(\varphi_{p2}-\varphi_{c2})}$, $\rho_{34} = \sigma_{34}e^{i(\varphi_{c2}-\varphi_{p1})}$, $\rho_{43} = \sigma_{43}e^{i(\varphi_{c1}-\varphi_{p2})}$, $\rho_{13} = \sigma_{13}e^{i\varphi_{c1}}$, $\rho_{14} = \sigma_{14}e^{i\varphi_{p2}}$, $\rho_{23} = \sigma_{23}e^{i\varphi_{p1}}$ and $\rho_{24} = \sigma_{24}e^{i\varphi_{c2}}$, where the relative phases are $\varphi_1 = \varphi_{p1} - \varphi_{c1}$ and $\varphi_2 = \varphi_{c2} - \varphi_{p2}$, satisfying $\varphi_{p1} - \varphi_{c1} = -(\varphi_{p2} - \varphi_{c2})$, $\varphi_{c2} - \varphi_{p1} = -(\varphi_{c1} - \varphi_{p2})$.

With the redefined density matrix elements, we obtain the following new equations:

$$\begin{aligned}
&\dot\sigma_{11} = iG_{c1}^*(x)\sigma_{31} - iG_{c1}(x)\sigma_{13} + iG_{p2}^*\sigma_{41} - iG_{p2}\sigma_{14} + \Gamma_{31}\sigma_{33} + \Gamma_{41}\sigma_{44} \\
&\dot\sigma_{12} = [i(\Delta_{c1} - \Delta_{p1}) - \gamma_{12}]\sigma_{12} + iG_{c1}^*(x)\sigma_{32} - iG_{p1}\sigma_{13} + iG_{p2}^*\sigma_{42} \\
&- iG_{c2}\sigma_{14} - (\eta_1\sqrt{\Gamma_{31}\Gamma_{32}}\cos\theta_1\sigma_{33} + \eta_2\sqrt{\Gamma_{41}\Gamma_{42}}\cos\theta_2\sigma_{44}) \\
&\dot\sigma_{13} = (i\Delta_{c1} - \gamma_{13})\sigma_{13} - iG_{c1}^*(x)\sigma_{11} - iG_{p1}^*\sigma_{12} + iG_{c1}^*(x)\sigma_{33} + iG_{p2}^*\sigma_{43} \\
&\dot\sigma_{14} = (i\Delta_{p2} - \gamma_{14})\sigma_{14} - iG_{p2}^*\sigma_{11} - iG_{c2}^*(x)\sigma_{12} + iG_{c1}^*(x)\sigma_{34} + iG_{p2}^*\sigma_{44} \\
&\dot\sigma_{22} = iG_{p1}^*\sigma_{32} - iG_{p1}\sigma_{23} + iG_{c2}^*(x)\sigma_{42} - iG_{c2}(x)\sigma_{24} + \Gamma_{32}\sigma_{33} + \Gamma_{42}\sigma_{44} \\
&\dot\sigma_{23} = (i\Delta_{p1} - \gamma_{23})\sigma_{23} - iG_{c1}^*(x)\sigma_{21} - iG_{p1}^*\sigma_{22} + iG_{p1}^*\sigma_{33} + iG_{c2}^*(x)\sigma_{43} \\
&\dot\sigma_{24} = (i\Delta_{c2} - \gamma_{24})\sigma_{24} - iG_{p2}^*\sigma_{21} - iG_{c2}^*(x)\sigma_{22} + iG_{p1}^*\sigma_{34} + iG_{c2}^*(x)\sigma_{44} \\
&\dot\sigma_{33} = iG_{c1}(x)\sigma_{13} - iG_{c1}^*(x)\sigma_{31} + iG_{p1}\sigma_{23} - iG_{p1}^*\sigma_{32} - \Gamma_{32}\sigma_{33} - \Gamma_{31}\sigma_{33} \\
&\dot\sigma_{34} = [i(\Delta_{p2} - \Delta_{c1}) - \gamma_{34}]\sigma_{34} + iG_{c1}(x)\sigma_{14} - iG_{p2}^*\sigma_{31} \\
&+ iG_{p1}\sigma_{24} - iG_{c2}^*(x)\sigma_{32}
\end{aligned} \tag{3}$$

Note that Eq. (3), which includes phases, is identical to Eq. (2) except that η_0 is replaced by $\eta_i = \eta_0 e^{i\varphi_i}$, while the complex Rabi frequencies are replaced by real ones. In the following discussion, we set $\varphi_1 = \varphi_2 = \varphi$ and $\theta_1 = \theta_2 = \theta$ for convenience. Here, we set $\Delta_{c1} = \Delta_{c2} = 0$, thus $\Delta_{p2} = -\Delta_{p1} = \Delta_p$ with the requirement of a balance FWM process $\Delta_{c1} + \Delta_{c2} + \Delta_{p2} + \Delta_{p1} = 0$.

The nonreciprocal reflections based on a broken spatial symmetry of susceptibility depend on the linear variation of coupling field intensity. Here, we set $\left|G_{c1}(x)\right|^2 = \left|G_{c10}\sin\theta\right|^2 k_1 x$ $(\left|G_{c2}(x)\right|^2 = \left|G_{c20}\sin\theta\right|^2 k_2 x)$. It is worth stressing that $x \in (0.02\ \mu\text{m}, L)$, L is the length of atomic medium. Thus, we can obtain σ_{32}, which is governed by the probe de-

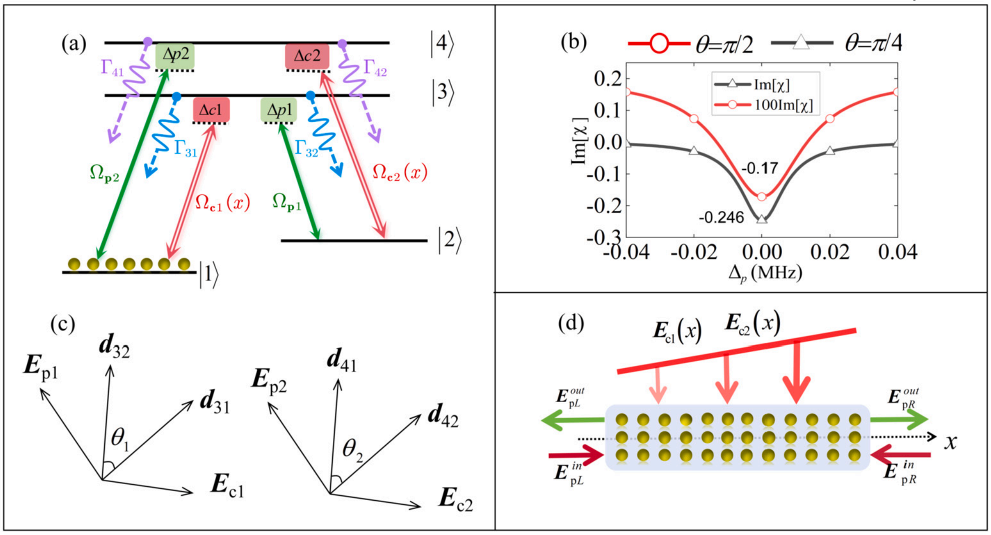

Fig. 1. (a) A four-level atomic system driven by two strong coupling fields and two weak probe fields. One laser field drives only a transition due to the chosen polarizations of relevant laser fields. The angle between the two dipole moments $\mathbf{d}_{31}$ and $\mathbf{d}_{32}$ ($\mathbf{d}_{41}$ and $\mathbf{d}_{42}$) is θ_1 (θ_2). (b) The imaginary part of the probe susceptibility Im$[\chi]$ is plotted against the detuning Δ_p for $\theta = \pi/2$ (red circles) and $\theta = \pi/4$ (black triangles) in the case of $\theta_1 = \theta_2 = \theta$ for convenience. (c) The diagram illustrates the uniform medium under illumination, where the coupling field is incident perpendicular to the x-direction and the probe is incident along the x-direction.

tuning Δ_p and position x. Correspondingly, the complex susceptibility of probe field yields χ_{pi} $(i = 1, 2)$

$$\chi_{p1}(\Delta_p, x) = \frac{N\left|\mathbf{d}_{32}\right|^2 \sigma_{32}(\Delta_p, x)}{\hbar\varepsilon_0\Omega_{p1}}, \tag{4}$$

$$\chi_{p2}(\Delta_p, x) = \frac{N\left|\mathbf{d}_{41}\right|^2 \sigma_{41}(\Delta_p, x)}{\hbar\varepsilon_0\Omega_{p2}}. \tag{5}$$

Here, ε_0 is the dielectric constant in vacuum, and the atomic density N is a constant. For $\chi_{p1}(\Delta_p, x)$ and $\chi_{p2}(\Delta_p, x)$ have the same variation of Δ_p, we only need to consider the propagation characteristics of one probe field as $\chi(\Delta_p, x)$, which can be shown clearly in Fig. 1(b).

In the following, we should check the light transport features, which can be examined by directly adopting standard transfer-matrix method [62,63]. First of all, we provide the jth 2×2 unimodular transfer matrix $m_j(\Delta_p, x_j)$ by dividing the whole sample of length L into S thin layers, $j \in (1, S)$. With identical thickness $\delta = L/S$, but the susceptibilities exhibit slight differences, which lead to variations in the transfer matrix

$$m_j(\Delta_p, x_j) = \frac{1}{t_j(\Delta_p, x_j)} \cdot \begin{bmatrix} (t_j(\Delta_p, x_j)^2 - r_j^r(\Delta_p, x_j) r_j^l(\Delta_p, x_j)) & r_j^l(\Delta_p, x_j) \\ -r_j^r(\Delta_p, x_j) & 1 \end{bmatrix} \tag{6}$$

with the corresponding right and left reflection and transmission complex amplitudes $r_j^{r,l}(\Delta_p, x_j)$ and $t_j^r(\Delta_p, x_j) = t_j^l(\Delta_p, x_j) = t_j(\Delta_p, x_j)$, respectively, determined by the complex refractive index $n_{p1}(\Delta_p, x_j) = \sqrt{1 + \chi_{p1}(\Delta_p, x_j)}$, $(n_{p2}(\Delta_p, x_j) = \sqrt{1 + \chi_{p2}(\Delta_p, x_j)})$. Then, we can write the total transfer matrices of j layers that probe light incidents from left-side, respectively

$$M^l(\Delta_p, j\delta) = m_1(\Delta_p, x_1) \times \ldots \times m_j(\Delta_p, x_j). \tag{7}$$

Note that $M^l(\Delta_p, j\delta)$ is multiplied from left to right by layers, and the opposite direction is multiplied from right to left. Thus, the probe reflectivities at jth layer that incident from the left-side are

$$R_j^l(\Delta_p, j\delta) = \left|r_j^l(\Delta_p, j\delta)\right|^2 = \left|\frac{M_{(12)}^l(\Delta_p, j\delta)}{M_{(22)}^l(\Delta_p, j\delta)}\right|^2 \tag{8}$$

with the complex amplitudes $r_j^{l,r}(\Delta_p, j\delta)$ and $t_j(\Delta_p, j\delta)$ determined by the transfer matrices can be clearly seen by Eq. (6). When $j = S$ the reflectivities and transmittivity at both ends of this finite atomic sample lead to the following expressions

$$R_i^l(\Delta_p, L) = \left|r_S^l(\Delta_p, L)\right|^2 = \left|\frac{M_{(12)}^l(\Delta_p, L)}{M_{(22)}^l(\Delta_p, L)}\right|^2, \tag{9}$$

$$R_i^r(\Delta_p, L) = \left|r_S^r(\Delta_p, L)\right|^2 = \left|\frac{M_{(21)}^l(\Delta_p, L)}{M_{(22)}^l(\Delta_p, L)}\right|^2. \tag{10}$$

With the Eq. (9)-(10), we can check the nonreciprocal even unidirectional reflections.

3. Numerical results and discussions

All of our discussions and results are based on the condition $\Delta_{c1} = \Delta_{c2} = 0$, $\Delta_{p1} = -\Delta_{p2} = \Delta_p$ and $G_{c10} = G_{c20} = G_{c0}$, $k_1 = k_2 = k$ for convenience. In the following, we will only check the right and left reflections of the probe field $\mathbf{E}_{p1}$ to simplify the problem, because $\mathbf{E}_{p2}$ should exhibit similar behaviors. We first examine the reflections of incident probe light from the right- and left-side, respectively, in the case $\theta = \pi/2$ (without SGC), as shown in Fig. 2(a). The probe light can be well reflected when incident from the right-side, and the maximum reflectivity R^r is over than 3.0, corresponding to the almost zero reflection of the left-side R^l in the frequency region $\Delta_p \in (0, 2$ MHz$)$. The physical essence of the formation of this wide and amplified unidirectional reflection band has two reasons: (I) The SLM of coupling fields can destroy the spatial symmetry of probe susceptibilities that induced the nonreciprocity of the left and right reflections, and most of the light entering from the left side is absorbed for the coupling field strength is too weak to cause quantum destructive interference at the front of medium (left-side), the probe light incident from right-side can be well reflected in the EIT window, for the intensity of coupling field reaches the maximum at the end of the sample (right-side). (II) The unidirectional reflections can be amplified during to the optical gain in the probe transitions via a resonant FWM process. Furthermore, we check one case with the presence of SGC that $\theta = \pi/4$, as shown in Fig. 2(b). There is an amplified narrow nonreciprocal reflection band of about 25 kHz, and the reflectivity of left-side has approached 3500 corresponding to the reflectivity

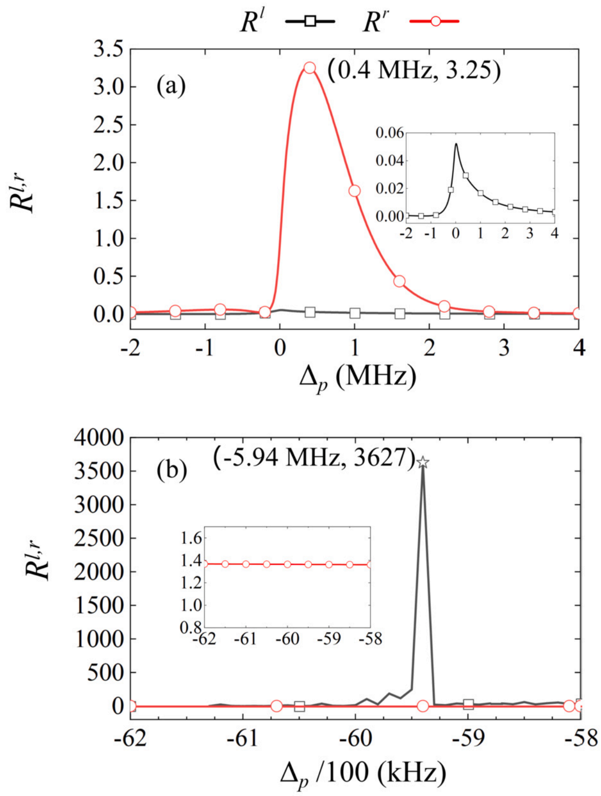

Fig. 2. The probe reflectivities $R^{l,r}$ *v.s.* detuning Δ_p with $\theta = \pi/2$ in (a) and $\theta = \pi/4$ in (b). Other parameters are $N = 3 \times 10^{12}$ cm^{-3}, $G_{c0} = 4$ MHz, $k = 1$ μm^{-1}, $G_{p1} = G_{p2} = 0.001$ MHz, $\Delta_{c1} = \Delta_{c2} = 0$, $\Gamma_{41} = \Gamma_{42} = \Gamma_{31} = \Gamma_{32} = 6$ MHz, $\varphi = 0$, $\mathbf{d}_{13} = 2.0 \times 10^{-29}$ C·m and the length $L = 4$ μm.

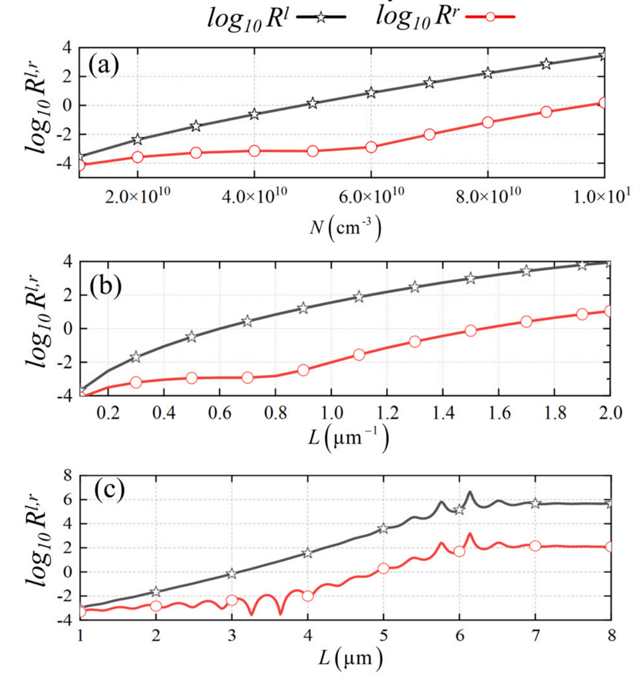

Fig. 3. The logarithm of the probe reflectivities ($\log_{10} R^{l,r}$) *v.s.* atomic density N, slope k and position x in (a), (b) and (c), respectively, with $\Delta_p = 0$ and $\theta = \pi/4$. Other parameters are the same as Fig. 2.

of right-side is just 1.4. Hence, one can see that SGC greatly enhances the reflection of probe light, for SGC can greatly enhance quantum coherence. While the nonreciprocity of left and right reflections has been reversed due to the phase variation caused by SGC. This is well demonstrated in Fig. 1(b), compared to the simple FWM resonance gain, the amplitude of the imaginary part of the susceptibility is increased by nearly 150 times with the contribution of both FWM and SGC. The results indicate that the presence of SGC plays a crucial role in enhancing the efficiency of the probe field gain during the FWM process.

Unfortunately, SGC reduces the unidirectionality of left and right reflections, as the left reflection is significantly increased while the right reflection is also slightly enhanced. To further optimize the nonreciprocal reflection, one feasible approach is to suppress the right reflection. This can be understood by examining the influence on reflectivity of relevant physical quantities, e.g., atomic number density N, the slope k and the length of medium L in Fig. 3. It is obvious, the reflections of left-side and right-side increase simultaneously with the increased N (k, and L), for they can enhance the probe susceptibility and the intensity of coupling fields. Considering the left reflectivity $R^l \gg 1$ and the right reflectivity $R^r \leq 10^{-2}$, we can assume that the probe field exhibits good unidirectionality and amplification. It is justified that the unidirectional reflection amplification can be realized with $N \in \left(6\times10^{10}\ \mathrm{cm}^{-3},\ 7\times10^{10}\ \mathrm{cm}^{-3}\right)$, $k \in \left(0.8\ \mu\mathrm{m}^{-1},\ 1.0\ \mu\mathrm{m}^{-1}\right)$, and $L \in (3.5\ \mu\mathrm{m}, 4.0\ \mu\mathrm{m})$. Then, we will choose the optimized parameters $N = 7 \times 10^{10}$ cm^{-3}, $k = 1$ μm^{-1} and $L = 4.0$ μm to check the nonreciprocity of amplified reflections with the relative phase φ and the dipole angle θ.

In particular, the requirement for the intensity of coupling fields can be reduced, because of the strong gain effect caused by the SGC effect. Then we reduce G_{c0} to 0.1 MHz, and with the relative phase $\varphi = 0$ to discuss the modulation of unidirectional reflection amplification by dipole angle θ, as depicted in Fig. 4. We first check the imaginary part of probe susceptibility with different dipole angles. Figs. 4(a1), 4(b1), 4(c1) and 4(d1) show that the gain amplitude of the imaginary part of the susceptibility increases more than 100 times, when θ changes from $\pi/2$ (without SGC) to $\pi/4$ (with SGC), which is in line with Fig. 1(b). However, there arose a strong absorption peak for $\theta = 3\pi/4$. When $\theta = \pi$, although the absorption weakens but still no gain appears. Correspondingly, we plot the probe reflectivities in Figs. 4(a2), 4(b2), 4(c2) and 4(d2). It is easy to see that the unidirectional reflection amplification formed only for $\theta = \pi/4$, when $\theta = \pi/2$ and $\theta = 3\pi/4$, the left and right reflections are nonreciprocal but with extremely low reflectivity, the nonreciprocity has completely disappeared for $\theta = \pi$. Thus, in order to examine the dipole angle on how to modulate the nonreciprocity and amplification of left and right reflections, we plot the imaginary part of the probe susceptibility varies both with θ and detuning Δ_p [see Fig. 4(e)]. The gain region appears in $0 < \theta < \pi/2$ and $-\pi/2 < \theta < 0$ around $\Delta_p = 0$. It is worth emphasizing that $\mathrm{Im}[\chi] = 0$ for $G_{ci}(x) = 0$, when $\theta = n\pi$. Furthermore, Fig. 4(f) exhibits that these two regions of dipole angle correspond to two amplified unidirectional reflection peaks for $\Delta_p = 0$, and the maximum value of the left reflectivity R^l appears at $\theta = \pi/5$.

Next, we set $\theta = \pi/5$ to explore the influence of relative phase φ on probe reflection. Figs. 5 (a1), (b1), (c1) and (d1) show that there is a gain peak around $\Delta_p = 0$ for $\varphi = 0$, corresponding to amplified unidirectional reflection peak [see Fig. 5(a2)]; and it reversed to absorption peak at $\varphi = \pi$, corresponding to extremely low nonreciprocal reflection [see Fig. 5(c2)]; The gain peak with weakening amplitude moves toward blue (red) detuning at $\varphi = \pi/2$ ($\varphi = 3\pi/2$), this insufficient gain amplitude resulted in the unidirectional reflection lower than 0.5 [see Figs. 5(b2) and 5(d2)]. It is because the probe gain can be periodically modulated by the relative phase φ, that the imaginary part of the susceptibility $\mathrm{Im}\left[\chi\right] < 0$ for $\varphi \in (-\pi/2 + 2n\pi,\ \pi/2 + 2n\pi)$, n is a positive integer, as depicted in Fig. 5(e). It is worth emphasizing, only when $\mathrm{Im}\left[\chi\right] < -0.2$ is sufficient to amplify the probe reflectivity and form amplified unidirectional reflection with $\varphi \in (-\pi/4 + 2n\pi,\ \pi/4 + 2n\pi)$, and the maximum value appears at $\varphi = 2n\pi$ [see Fig. 5(f)].

Last, we further investigate the parameters of relative phase φ and dipole angle θ to optimize the unidirectional reflection amplification. Fig. 6 (a) depicts that $\varphi \in (-\pi/4,\ \pi/4)$ corresponds to two amplified re-

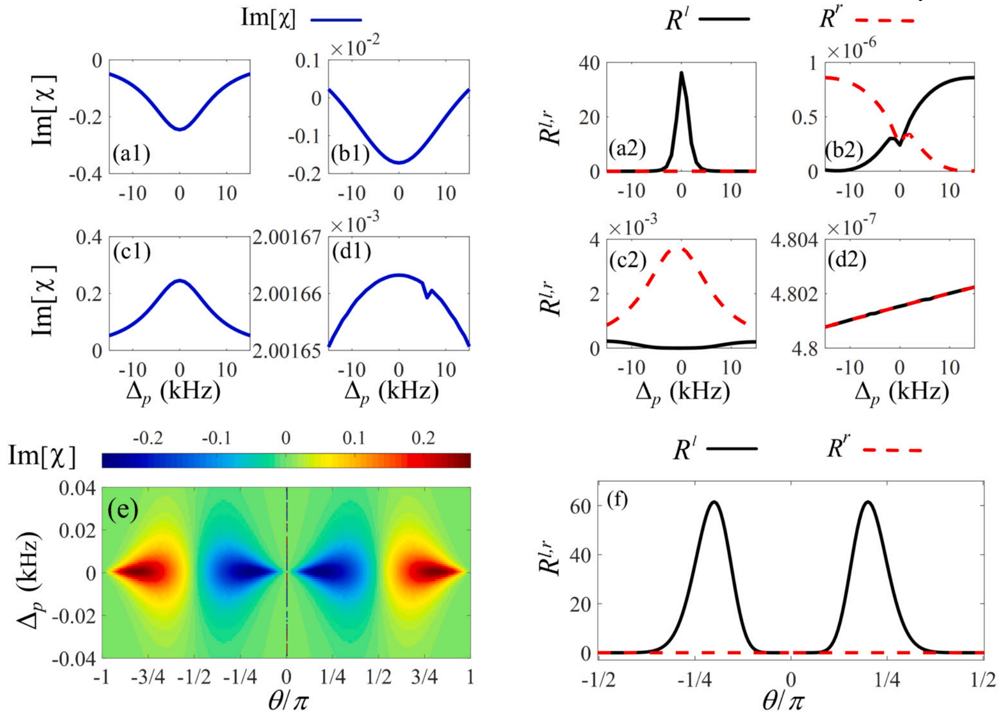

Fig. 4. Imaginary part of the probe susceptibility Im[χ] *v.s.* detuning Δ_p in (a1), (b1), (c1) and (d1). The reflectivities $R^{l,r}$ *vs*. detuning Δ_p in (a2), (b2), (c2) and (d2), with $\theta = \pi/4$ in (a*i*), $\theta = \pi/2$ in (b*i*), $\theta = 3\pi/4$ in (c*i*) and $\theta = \pi$ in (d*i*), $i = 1, 2$. Imaginary part of the probe susceptibility Im[χ] *v.s.* detuning Δ_p and the angle θ between dipole moments in (e). The reflectivities $R^{l,r}$ *v.s.* dipole moment angle θ in (f). Here $N = 7 \times 10^{10}$ cm^{-3}, $G_{c0} = 0.1$ MHz, $k = 1$ μm^{-1} and other parameters are the same as Fig. 2.

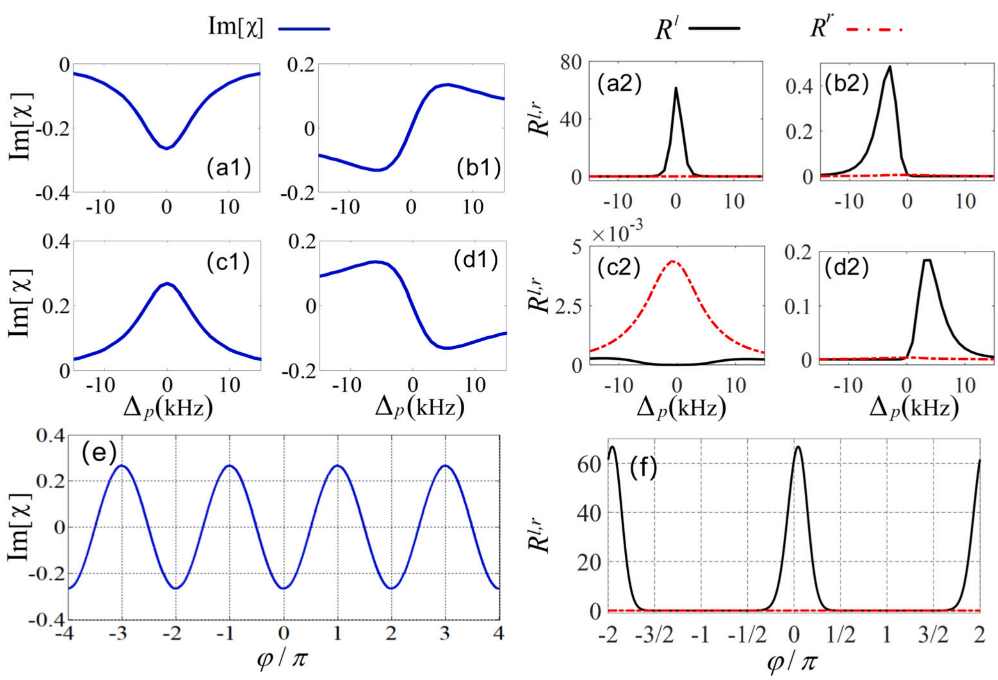

Fig. 5. Imaginary part of the probe susceptibility Im[χ] *v.s.* detuning Δ_p in (a1), (b1), (c1) and (d1). The reflectivities $R^{l,r}$ *v.s.* detuning Δ_p in (a2), (b2), (c2) and (d2), with $\varphi = 0$ in (a*i*), $\varphi = \pi/2$ in (b*i*), $\varphi = \pi$ in (c*i*) and $\varphi = 3\pi/2$ in (d*i*), $i = 1, 2$. Imaginary part of the probe susceptibility Im[χ] *v.s.* phase φ in (e). The reflectivities $R^{l,r}$ *v.s.* phase φ in (f). Here $\theta = \pi/5$ and other parameters are the same as Fig. 4.

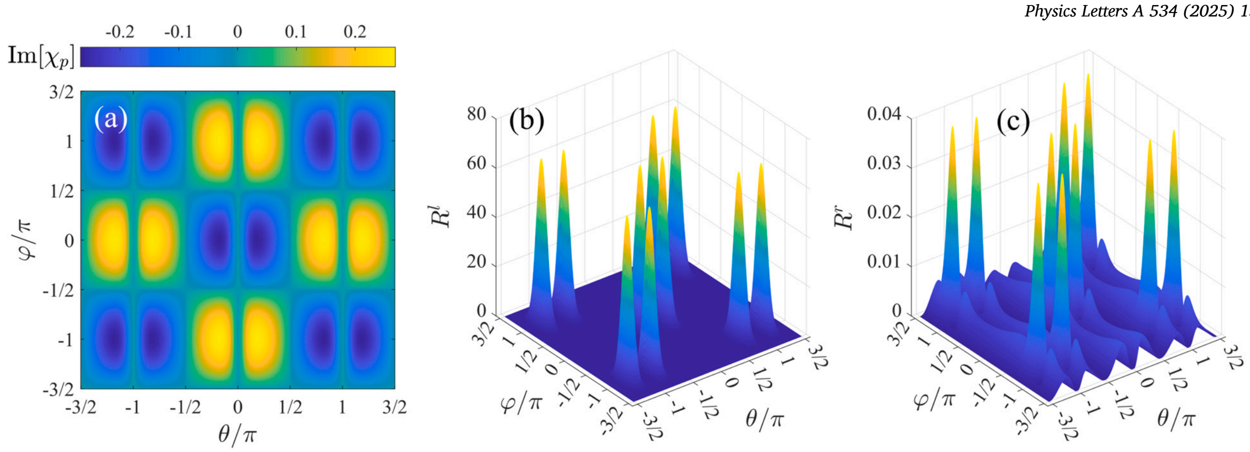

Fig. 6. Imaginary part of the probe susceptibility Im[χ] $v.s.$ the dipole moment angle θ and phase φ in (a). The left-side reflectivity R^l and right-side reflectivity R^r of the probe $v.s.$ the dipole moment angle θ and phase φ in (b) and (c). Here $\Delta_p = 0$ and other parameters are the same as Fig. 4.

gions (Im$[\chi] < -0.2$) of the dipole angle $-\pi/4 < \theta < 0$ and $0 < \theta < \pi/4$, while $\varphi \in (3\pi/4,\ 5\pi/4)$ [$\varphi \in (-5\pi/4,\ -3\pi/4)$] corresponds to four amplified regions of the dipole angle $-5\pi/4 < \theta < -\pi$, $-\pi < \theta < -3\pi/4$, $3\pi/4 < \theta < \pi$ and $\pi < \theta < 5\pi/4$. This strictly leads to the amplified unidirectional reflection, which can be displayed in Figs. 6(c) and 6(d) for the left reflectivity R^l can reach to 60 and the right reflectivity R^r is lower than 0.04. This implies that the amplified unidirectional reflection can be modulated accurately and freely by reasonable settings of relative phase φ and dipole angle θ.

4. Conclusion

In this paper, we demonstrated that a dramatically enhanced and narrowed unidirectional reflection can be achieved based on the combination of FWM, SGC, and SLM. The numerical results show that the FWM process can produce a wide and amplified unidirectional reflection band. However, after considering the SGC effect, the amplified reflectivity increased by several thousand times, and the nonreciprocity of left- and right-reflection is reversed, while the linewidth of reflection band narrowed to kHz, but the unidirectionality is weakened. Fortunately, an amplified unidirectional reflection band with amplitude over than 60 and linewidth of 10 kHz can be achieved by optimizing the corresponding parameters, such as atomic number density N, the slope k, the length of medium L, and which can be modulated by the relative phase φ and dipole angle θ. It is also worth noting that SGC in our atomic system not only greatly reduces the requirements on atomic sample density and coupling field intensities, but also provides a flexible phase control for reversing the amplified and vanishing reflectivities. The two effects of FWM and SGC have been extensively and thoroughly studied before, while not together yet in order to utilize their respect advantages, our results demonstrate that the combination of the two can enhance the quantum interference. It is worth emphasizing that the existence condition of SGC is very strict. However, the latest experiment in atomic ensembles has observed vacuum induced quantum beats [45], which provides more possibilities for our theoretical work. In addition, the efficient coupling between the four waves may occur when momentum is conserved for a phase matching, which can be realized by setting up two pairs of backpropagation laser fields. In summary, our theoretical proposal is feasible in experiment. Especially, the amplified narrow band yields low out-of-band noise. Thus, our results pave a way to design high-quality nonreciprocal devices which could prove advantageous for many on-chip functionalities.

CRediT authorship contribution statement

Yue Geng: Data curation, Conceptualization. **Chen Peng:** Software. **Xinfu Zheng:** Software, Resources. **Dong Yan:** Validation. **Hanxiao Zhang:** Formal analysis. **Jinhui Wu:** Methodology, Formal analysis. **Hong Yang:** Writing – review & editing, Writing – original draft, Supervision, Resources, Investigation, Formal analysis.

Declaration of competing interest

The authors declare no conflicts of interest.

Acknowledgements

This work is supported by the Hainan Provincial Natural Science Foundation of China (Grant Nos. 122QN302, 121MS033) and the National Natural Science Foundation of China (Grant Nos. 12204137, 12126314, 12126351). This project is also supported by the specific research fund of the Innovation Platform for Academicians of Hainan Province (Grant Nos. YSPTZX202215, YSPTZX202207), the Hainan Provincial Banyan Tree Foundation (Grant Nos. RSYH20231165828X, RSYH20231165827X), Key Laboratory of Laser Technology and Optoelectronic Functional Materials of Hainan Province.

Data availability

No data was used for the research described in the article.

References

[1] S. Yuan, L. Chen, Z. Wang, W. Deng, Z. Hou, C. Zhang, Y. Yu, X. Wu, X. Zhang, On-chip terahertz isolator with ultrahigh isolation ratios, Nat. Commun. 12 (2021) 5570.
[2] X.-W. Xu, Y. Li, Optical nonreciprocity and optomechanical circulator in three-mode optomechanical systems, Phys. Rev. A 91 (2015) 053854.
[3] C. Sayrin, C. Junge, R. Mitsch, B. Albrecht, D. O'Shea, P. Schneeweiss, J. Volz, A. Rauschenbeutel, Nanophotonic optical isolator controlled by the internal state of cold atoms, Phys. Rev. X 5 (2015) 041036.
[4] Y.-Q. Hu, Y.-H. Qi, Y. You, S.-C. Zhang, G.-W. Lin, X.-L. Li, J.-B. Gong, S.-Q. Gong, Y.-P. Niuet, Passive nonlinear optical isolators by passing dynamic reciprocity, Phys. Rev. A 16 (2021) 01404.
[5] M. Scheucher, A. Hilico, E. Will, J. Volz, A. Rauschenbeutel, Quantum optical circulator controlled by a single chirally coupled atom, Science 354 (2016) 1577.
[6] A. Kamal, A. Metelmann, Minimal models for non-reciprocal amplification using biharmonic drives, Phys. Rev. Appl. 7 (2017) 034031.
[7] R. Peng, W.-Z. Zhang, S.-L. Chao, C.-S. Zhao, Z. Yang, J.-Y. Yang, L. Zhou, Unidirectional amplification in optomechanical system coupling with a structured bath, Opt. Express 30 (2022) 21649.
[8] B. Abdo, K. Sliwa, L. Frunzio, M. Devoret, Directional amplification with a Josephson circuit, Phys. Rev. X 3 (2013) 031001.
[9] B. Abdo, K. Sliwa, S. Shankar, M. Hatridge, L. Frunzio, R. Schoelkopf, M. Devoret, Josephson directional amplifier for quantum measurement of super conducting circuits, Phys. Rev. Lett. 112 (2014) 167701.
[10] T.T. Koutserimpas, R. Fleury, Nonreciprocal gain in non-Hermitian time Floquet systems, Phys. Rev. Lett. 120 (2018) 087401.

[11] C. Li, L. Jin, Z. Song, Non-Hermitian interferometer: unidirectional amplification without distortion, Phys. Rev. A 95 (2017) 022125.
[12] L. Jin, Asymmetric lasing at spectral singularities, Phys. Rev. A 97 (2018) 033840.
[13] D.V. Novitsky, A. Karabchevsky, A.V. Lavrinenko, A.S. Shalin, A.V. Novitsky, PT-symmetry breaking in multilayers with resonant loss and gain locks light propagation direction, Phys. Rev. B 98 (2018) 125102.
[14] N.T. Otterstrom, E.A. Kittlaus, S. Gertler, R.O. Behunin, A.L. Lentine, P.T. Rakich, Resonantly enhanced nonreciprocal silicon Brillouin amplifier, Optica 6 (2019) 1117.
[15] E.A. Kittlaus, H. Shin, P.T. Rakich, Large Brillouin amplification in silicon, Nat. Photonics 10 (2016) 463.
[16] N.T. Otterstrom, R.O. Behunin, E.A. Kittlaus, Z. Wang, P.T. Rakich, A silicon Brillouin laser, Science 360 (2018) 1113.
[17] Y. Souidi, F. Taleb, J. Zheng, M.W. Lee, F.D. Burck, V. Roncin, Low-noise and high-gain Brillouin optical amplifier for narrowband active optical filtering based on a pump-to-signal optoelectronic tracking, Appl. Opt. 55 (2016) 248.
[18] Z.-Y. Wang, J. Qian, Y.-P. Wang, J. Li, J.-Q. You, Realization of the unidirectional amplification in a cavity magnonic system, Appl. Phys. Lett. 123 (2023) 153904.
[19] L.M. de Lepinay, E. Damskagg, C.F. Ockeloen-Korppi, M.A. Sillanpaa, Realization of directional amplification in a microwave optomechanical device, Phys. Rev. Appl. 11 (2019) 034027.
[20] B. Peng, S.K. Ozdemir, F. Lei, F. Monifi, M. Gianfreda, G.-L. Long, S. Fan, F. Nori, C.M. Bender, L. Yang, Parity–time-symmetric whispering-gallery microcavities, Nat. Phys. 10 (2014) 394.
[21] L.-N. Song, Q. Zheng, X.-W. Xu, C. Jiang, Y. Li, Optimal unidirectional amplification induced by optical gain in optomechanical systems, Phys. Rev. A 100 (2019) 043835.
[22] Y. Jiang, S. Maayani, T. Carmon, F. Nori, H. Jing, Nonreciprocal phonon laser, Phys. Rev. Appl. 10 (2018) 064037.
[23] H. Lu, S.K. Ozdemir, L.-M. Kuang, F. Nori, H. Jing, Exceptional points in random-defect phonon lasers, Phys. Rev. Appl. 8 (2017) 044020.
[24] A.M. de las Heras, I. Carusotto, Unidirectional lasing in nonlinear Taiji microring resonators, Phys. Rev. A 104 (2021) 043501.
[25] D. Malz, L.D. Toth, N.R. Bernier, A.K. Feofanov, T.J. Kippenberg, A. Nunnenkamp, Quantum-limited directional amplifiers with optomechanics, Phys. Rev. Lett. 120 (2018) 023601.
[26] C.-S. Zhao, R. Peng, Z. Yang, S.-L. Chao, C. Li, Z.-H. Wang, L. Zhou, Nonreciprocal amplification in a cavity magnonics system, Phys. Rev. A 105 (2022) 023709.
[27] Y.-W. Jing, H.-Q. Shi, X.-W. Xu, Nonreciprocal photon blockade and directional amplification in a spinning resonator coupled to a two-level atom, Phys. Rev. A 104 (2021) 033707.
[28] A. Metelmann, A.A. Clerk, Nonreciprocal photon transmission and amplification via reservoir engineering, Phys. Rev. X 5 (2015) 021025.
[29] A. Kamal, A. Metelmann, Minimal models for nonreciprocal amplification using biharmonic drives, Phys. Rev. Appl. 7 (2017) 034031.
[30] L.-N. Song, Z.-H. Wang, Y. Li, Enhancing optical nonreciprocity by an atomic ensemble in two coupled cavities, Opt. Commun. 415 (2018) 39.
[31] G.-W. Lin, S.-C. Zhang, Y.-Q. Hu, Y.-P. Niu, J.-B. Gong, S.-Q. Gong, Nonreciprocal amplification with four-level hot atoms, Phys. Rev. Lett. 123 (2019) 033902.
[32] H. Yang, S.-C. Zhang, Y.-P. Niu, S.-Q. Gong, Ultra-strong nonreciprocal amplification with hot atoms, Opt. Commun. 515 (2022) 128195.
[33] Y. Geng, X.-S. Pei, G.-R. Li, X.-Y. Lin, H.-X. Zhang, D. Yan, H. Yang, Spatial susceptibility modulation and controlled unidirectional reflection amplification via four-wave mixing, Opt. Express 31 (2023) 38228–38239.
[34] G.-R. Li, Y. Geng, X.-S. Pei, J.-H. Wu, X.-Y. Lin, D. Yan, H.-X. Zhang, H. Yang, Phase and detuning control of the unidirectional reflection amplification based on the broken spatial symmetry, Opt. Express 32 (2024) 12839.
[35] H. Yang, T.-G. Zhang, Y. Zhang, Probe gain via four-wave mixing based on spontaneously generated coherence, Chin. Phys. B 26 (2017) 024204.
[36] A. Schilke, C. Zimmermann, P.W. Courteille, W. Guerin, Optical parametric oscillation with distributed feedback in cold atoms, Nat. Photonics 6 (2012) 101–104.
[37] Y.-P. Zhang, Z.-G. Wang, Z.-Q. Nie, C.-B. Li, H.-X. Chen, K.-Q. Lu, M. Xiao, Four-wave mixing dipole soliton in laser-induced atomic gratings, Phys. Rev. Lett. 106 (2011) 093904.
[38] T. Shui, W.-X. Yang, M.-T. Cheng, R.K. Lee, Optical nonreciprocity and nonreciprocal photonic devices with directional four-wave mixing effect, Opt. Express 30 (2022) 6284.
[39] D. Wang, W.-Q. Lu, J.-Y. Han, Y. Zhang, Y. Liu, H.-T. Zhou, J.-Z. Wu, J.-X. Zhang, Near-resonant twin-beam generation from degenerate four-wave mixing in hot ^{133}Cs vaporenabled by field-dressed energy levels, Opt. Express 31 (2023) 38255.
[40] H.-M. Zhao, X.-J. Zhang, M. Artoni, G.C. La Rocca, J.-H. Wu, Nonlocal Rydberg enhancement for four-wave-mixing biphoton generation, Phys. Rev. A 109 (2024) 043711.
[41] H. Yang, T.-G. Zhang, X. Zou, Y. Zhang, Inversionless gain via six-wave mixing and the investigation of distributed feedback, Phys. Lett. A 381 (2017) 1620.
[42] K.-K. Li, J.-M. Wen, Y. Cai, S.V. Ghamsari, C.-B. Li, F. Li, Z.-Y. Zhang, Y.-P. Zhang, M. Xiao, Direct generation of time-energy-entangled W triphotons in atomic vapor, Sci. Adv. 10 (2024) eado3199.
[43] Z.-M. Wu, J.-H. Li, Y. Wu, Phase-engineered photon correlations in weakly coupled nanofiber cavity QED, Phys. Rev. A 109 (2024) 033709.
[44] Z.-M. Wu, J.-H. Li, Y. Wu, Vacuum-induced quantum-beat-enabled photon antibunching, Phys. Rev. A 108 (2023) 023727.
[45] H.S. Han, A. Lee, K. Sinha, F.K. Fatemi, S.L. Rolston, Observation of vacuum-induced collective quantum beats, Phys. Rev. Lett. 127 (2021) 073604.
[46] A.-J. Li, J.-Y. Gao, J.-H. Wu, L. Wang, Simulating spontaneously generated coherence in a four-level atomic system, J. Phys. B, At. Mol. Opt. Phys. 38 (2005) 3815.
[47] C.-L. Wang, Z.-H. Kang, S.-C. Tian, J.-H. Wu, Control of spontaneous emission from a micro-wave driven atomic system, Opt. Express 20 (2012) 3509.
[48] W.-H. Xu, J.-Y. Gao, Gain spectrum of a laser-driven Λ-type atom with vacuum-induced coherence, J. Opt. Soc. Am. B 22 (2005) 2385.
[49] J.-H. Wu, J.-Y. Gao, Phase control of light amplification without inversion in a Λ system with spontaneously generated coherence, Phys. Rev. A 65 (2002) 063807.
[50] M.V. Gurudev Dutt, J. Cheng, B. Li, X.-D. Xu, X.-Q. Li, P.R. Berman, D.G. Steel, A.S. Bracker, D. Gammon, S.E. Economou, R.-B. Liu, L.J. Sham, Stimulated and spontaneous optical generation of electron spin coherence in charged GaAs quantum dots, Phys. Rev. Lett. 94 (2005) 227403.
[51] Y. Zhang, Y.-M. Liu, T.-Y. Zheng, J.-H. Wu, Light reflector, amplifier, and splitter based on gain-assisted photonic band gaps, Phys. Rev. A 94 (2016) 013836.
[52] C.-L. Wang, A.-J. Li, X.-Y. Zhou, Z.-H. Kang, J. Yun, J.-Y. Gao, Investigation of spontaneously generated coherence in dressed states of ^{85}Rb atoms, Opt. Lett. 33 (2008) 687.
[53] D.G. Norris, L.A. Orozco, P. Barberis-Blostein, H.J. Carmichael, Observation of ground-state quantum beats in atomic spontaneous emission, Phys. Rev. Lett. 105 (2010) 123602.
[54] Y. Lien, G. Barontini, M. Scheucher, M. Mergenthaler, J. Goldwin, E.A. Hinds, Observing coherence effects in an overdamped quantum system, Nat. Commun. 7 (2016) 13933.
[55] J.-H. Wu, M. Artoni, G.C. La Rocca, Perfect absorption and no reflection in disordered photonic crystals, Phys. Rev. A 95 (2017) 053862.
[56] J.-H. Wu, M. Artoni, G.C. La Rocca, Parity-time-antisymmetric atomic lattices without gain, Phys. Rev. A 91 (2015) 033811.
[57] C. Hang, G.-X. Huang, V.V. Konotop, Pt symmetry with a system of three-level atoms, Phys. Rev. Lett. 110 (2013) 083604.
[58] Y. Zhang, J.-H. Wu, M. Artoni, G.C. La Rocca, Controlled unidirectional reflection in cold atoms via the spatial Kramers-Kronig relation, Opt. Express 29 (2021) 5890–5900.
[59] S. Horsley, M. Artoni, G.C. La Rocca, Spatial Kramers–Kronig relations and the reflection of waves, Nat. Photonics 9 (2015) 436–439.
[60] D. Ye, C. Cao, T. Zhou, J. Huangfu, G. Zheng, L. Ran, Observation of reflectionless absorption due to spatial Kramers-Kronig profile, Nat. Commun. 8 (2017) 51.
[61] Y.-X. Wang, Y. Zhang, L. Du, J.-H. Wu, Chiral phase modulation and a tunable broadband perfect absorber using a coherent cold atomic ensemble, Phys. Rev. A 108 (2023) 053716.
[62] M. Artoni, G.C. La Rocca, F. Bassani, Resonantly absorbing one-dimensional photonic crystal, Phys. Rev. E 72 (2005) 046604.
[63] Y. Zhang, Y. Xue, G.g. Wang, C.-L. Cui, R. Wang, J.-H. Wu, Steady optical spectra and light propagation dynamics in cold atomic samples with homogeneous or inhomogeneous densities, Opt. Express 19 (2011) 2111–2119.